11-2-2004

The ACS Virgo Cluster Survey. II. Data Reduction Procedures

Andrés Jordán
Rutgers University

John P. Blakeslee
The Johns Hopkins University

Eric W. Peng
Rutgers University

Simona Mei
The Johns Hopkins University

Patrick Côté
Rutgers University

See next page for additional authors

Accepted for publication in ApJS

The ACS Virgo Cluster Survey II. Data Reduction Procedures[1]

Andrés Jordán[2,3], John P. Blakeslee[4], Eric W. Peng[2], Simona Mei[4], Patrick Côté[2], Laura Ferrarese[2], John L. Tonry[5], David Merritt[6], Miloš Milosavljević[7,8], and Michael J. West[9]

ABSTRACT

The ACS Virgo Cluster Survey is a large program to carry out multi-color imaging of 100 early-type members of the Virgo Cluster using the Advanced Camera for Surveys (ACS) on the *Hubble Space Telescope*. Deep F475W and F850LP images ($\approx$ SDSS g and z) are being used to study the central regions of the program galaxies, their globular cluster systems, and the three-dimensional structure of Virgo itself. In this paper, we describe in detail the data reduction procedures used for the survey, including image registration, drizzling strategies, the computation of weight images, object detection, the identification of globular cluster candidates, and the measurement of their photometric and structural parameters.

---

[1]Based on observations with the NASA/ESA *Hubble Space Telescope* obtained at the Space Telescope Science Institute, which is operated by the Association of Universities for Research in Astronomy, Inc., under NASA contract NAS 5-26555

[2]Department of Physics and Astronomy, Rutgers University, Piscataway, NJ 08854; andresj@physics.rutgers.edu, ericpeng@physics.rutgers.edu, pcote@physics.rutgers.edu, lff@physics.rutgers.edu

[3]Claudio Anguita Fellow

[4]Department of Physics and Astronomy, Johns Hopkins University, Baltimore, MD 21218; jpb@pha.jhu.edu, smei@pha.jhu.edu

[5]Institute of Astronomy, University of Hawaii, 2680 Woodlawn Drive, Honolulu, HI 96822; jt@ifa.hawaii.edu

[6]Department of Physics, Rochester Institute of Technology, 84 Lomb Memorial Drive, Rochester, NY 14623; merritt@mail.rit.edu

[7]Theoretical Astrophysics, California Institute of Technology, Pasadena, CA 91125; milos@tapir.caltech.edu.

[8]Sherman M. Fairchild Fellow

[9]Department of Physics & Astronomy, University of Hawaii, Hilo, HI 96720; westm@hawaii.edu.

Subject headings: methods: data analysis — techniques: image processing — astronomical data bases: surveys — galaxies: clusters: individual (Virgo)

1. Introduction

The Virgo Cluster is the largest concentration of early-type galaxies in the Local Supercluster. As such, it has played a central role in understanding how these galaxies form and evolve in dense environments, providing invaluable information on the extragalactic distance scale, the nature of galactic nuclei, globular cluster systems, and the shape and universality of the galactic luminosity function. Indeed, the population of early-type Virgo galaxies has been the target of several thousand observations with the *Hubble Space Telescope* (HST) since its launch in 1990.

In the eleventh HST observing cycle, we initiated the ACS Virgo Cluster Survey (Côté et al. 2004; hereafter Paper I), a program to acquire F475W ($\approx$ SDSS g) and F850LP ($\approx$ SDSS z) images for 100 early-type members of Virgo using the *Advanced Camera for Surveys* (ACS; Ford et al. 1998). Paper I of this series describes the survey itself, including a brief overview of the scientific goals, the selection of the program galaxies and their ensemble properties, the choice of filters, the field placement and orientation, and the anticipated sensitivity limits.

It is the aim of the ACS Virgo Cluster Survey to use a single, homogeneous dataset to measure surface brightness fluctuation (SBF) distances, study the globular cluster systems, and examine the central structure of 100 early-type members of the Virgo Cluster. Both the scope of the survey — consisting of 500 ACS images spread over 100 separate fields — and its multiple scientific goals require an automated and flexible data reduction procedure. In this paper, we describe the pipeline used in the reduction and analysis of the ACS imaging for this survey. As discussed in Paper I, the ACS Virgo Cluster Survey also includes a substantial coordinated parallel component, consisting of WFPC2 imaging for 100 "intergalactic" fields in Virgo; a complete discussion of the reduction and analysis of these parallel data will be given in a separate paper. Similarly, future papers in this series will present additional details on the isophotal, globular cluster and SBF analyses.

2. Data Reduction Procedures

2.1. Observations

The program (GO-9401) consists of ACS imaging for 100 confirmed members of the Virgo Cluster having morphological types E, S0, dE, dE,N or dS0. The program galaxies span a factor of ≈ 450 in blue luminosity: i.e., $9.31 \leq B_T \leq 15.97$. The 21 brightest program galaxies constitute a complete sample of Virgo galaxies brighter than $B_T = 12$, while the full sample includes nearly half of all early-type members of Virgo with $B_T < 16$.

Observations for each program galaxy were carried out within a single orbit with HST, using the ACS Wide Field Channel (WFC). This camera consists of two butted 2048×4096 CCD detectors (15μm pixels) having spectral response in the range 0.35–1.05μm. With a scale of 0.049 arcsec per pixel, the camera has a $202'' \times 202''$ field of view. The center of each galaxy was positioned near the WFC aperture, at pixel position (2096, 200) on the WFC1 detector, and then offset perpendicular to the gap between the WFC1 and WFC2 detectors. For the 12 brightest galaxies, this offset was $10''$. An offset of $5''$ was applied to the remaining galaxies.

An identical observing sequence was adopted for each galaxy: *i.e.*, two 375 sec exposures in the F475W filter (750 sec in total), two 560 sec exposures in the F850LP filter, and a single 90 sec exposure in F850LP (1210 sec in total). For several of the program galaxies, the central surface brightness in the redder bandpass can approach $\mu_z \simeq 12$ mag arcsec^{-2}, so this 90 sec F850LP exposure was required to repair nuclei saturated in the deep F850LP images. The entire dataset for each galaxy therefore consists of an identical set of five images, which were reduced and analyzed as described below. These reduction procedures are summarized in schematic form by the flowchart shown in Figure 1.

Table 1 gives the observing log for all ACS observations related to program GO-9401. From left to right, the columns of this table record the identification number of each program galaxy, the Virgo Cluster Catalog number from Binggeli, Sandage & Tammann (1985), the universal date of start of the observation, the dataset name, the universal time at the start of the observation and the position angle, Θ, of the y axis of the WFC1 detector. The final two columns give the exposure time and filter for each observation.

2.2. Source Matching and Image Registration

The imaging for each program galaxy was completed in a single orbit — at fixed telescope position and roll angle — so the images for each galaxy are expected to be closely registered.

Nevertheless, small offsets might be present, so shifts between the images were measured using the method described in Blakeslee et al. (2003). A brief overview of this method is given below.

To determine the shifts ($\Delta x,\ \Delta y$) and rotations between the various images, SExtractor (Bertin & Arnout 1996) was run with a signal-to-noise threshold of S/N = 10 on both science extensions for each image.[1] The resultant catalogs were trimmed on the basis of object size and shape parameters, thereby rejecting the vast majority of cosmic rays, CCD artifacts, and diffuse extended objects. If fewer than ten "good" sources remained, SExtractor was rerun at a lower threshold. The (x, y) coordinates of each source were then corrected using the distortion model read from the IDCTAB FITS table specified in the image headers. For each observation, sources in the two CCD chips were placed on a common rectified frame using the IDCTAB parameters V2REF and V3REF.

The MATCH program of Richmond et al. (2000), which is based on the triangle-based search algorithm of Valdes et al. (1995), was used to derive shifts and rotations with respect to a reference image. By default, this reference image was taken to be the one having the greatest number of detected sources. The MATCH program was modified to accept an input guess for the transformation (derived from the headers) and report additional diagnostics to aid in evaluating the success of the matching. The complete catalog of sources was then used to fine tune this initial transformation.

This exercise revealed the measured rotations to be negligibly small in all cases, so we simply evaluated the median ($\Delta x,\ \Delta$y) shifts for the full list of matched sources. The median shifts measured for the images were typically $\lesssim 0.2$ pixel.

2.3. Drizzling

With the offsets determined in this way, the images were combined using the PYRAF task *multidrizzle* (Koekemoer et al. 2002). Since several of the program galaxies fill a significant fraction of the field of view (*i.e.*, the brightest galaxies have effective radii $r_e \gtrsim 1'$), the task was run without sky subtraction. Cosmic ray rejection was performed using this task; after some experimentation, the relevant parameters in the task *driz_cr* were set to `scale = '1.7 0.7'` and `snr = '4.5 2.0'`. The drizzled images have dimension 4256×4256 pixels for all galaxies.

Given the differing requirements of the various scientific programs, both `Lanczos3` and

[1]There are two such extensions (*i.e.*, CCD detectors) for the Wide Field Channel on ACS.

`Gaussian` kernels were used to distribute flux onto the output image, thereby producing two independent image sets for each galaxy. For the globular cluster and SBF analysis, images were generated using a `Lanczos3` kernel, which reduces the correlation between output pixels (and thus produces images with better noise characteristics for SBF analysis). As a drawback, the negative lobes of this kernel make the repair of bad pixels less effective. This is a potentially significant problem for the measurement of surface brightness profiles in the innermost regions of the program galaxies. Thus, the `Gaussian` kernel was used to create the drizzled images used in the isophotal analysis of the program galaxies.

In order to repair bad pixels, the `bits` parameter is set to indicate which pixels are to be considered good based on their value in the data quality file and thus drizzled into the final image. For isophotal analysis, we set `bits=8322`, which allows for the rejection of saturated pixels (*i.e.*, saturated pixels are not drizzled and the final value in the drizzled image is obtained by scaling based on the good pixels). Due to the difficulty in repairing bad pixels with the `Lanczos3` kernel, we set `bits=8576`, which allows the flux from saturated pixels to be drizzled onto the final images.

2.4. Weight Images

Weight images were constructed in order to perform object detection and to aid in the determination of photometric and structural parameters for the globular cluster candidates (see §2.6). The presence of a strong signal arising from the SBF of the program galaxies — particularly in the z band — requires that the "noise" contributed by the SBF must be included in the weight images in order to avoid the detection of spurious sources corresponding to real fluctuations in the underlying stellar populations.

In constructing the weight images, we begin with the WHT images, H_{ij}, produced by *multidrizzle*, in which each pixel contains the effective exposure time: *i.e.*, the total time during which photons contributing to observed counts were collected. The instrumental variance, I_{ij}, is then calculated as

$$I_{ij} = f_1 T + f_2 r^2 \tag{1}$$

where T is the exposure time and $r = 5e^-$ is the detector readnoise for WFC/ACS. The factors f_1 and f_2 were determined empirically by comparing the resulting variance images calculated using the above expression with the noise measured directly in exposures of varying duration drawn from the ACS Early Release Observations. The values determined in this way were $f_1 = 0.02222$ and $f_2 = 1.38$. With the instrumental noise properties in hand, weight

(inverse variance second^{-2}) images consisting of Poisson and readnoise were calculated as

$$W_{ij} = TH_{ij}(TD_{ij} + I_{ij})^{-1} \tag{2}$$

where D_{ij} denotes the data image in electrons second^{-1}. Weight images in this form are then used in the measurement of photometric and structural parameters for the globular cluster candidates, as described in §2.6.

As noted above, it is important to include the contribution of SBF "noise" when performing object detection. The ratio of the variance from SBF, σ_L^2, to that of the Poisson noise from the galaxy, σ_p^2 is given by (Tonry & Schneider 1988)

$$\frac{\sigma_L^2}{\sigma_p^2} = 10^{-0.4(\overline{m}-m_{\rm zpt*})} \tag{3}$$

where

$$\overline{m} \equiv -2.5\log(\sigma_L^2/O_{ij}) + m_{zpt*}$$

is the fluctuation magnitude in the given band, $O_{ij} \equiv \sigma_p^2$ is the mean intensity of the galaxy, and

$$m_{zpt*} = m_{zpt} + 2.5\log(T).$$

Here m_{zpt} is the photometric zeropoint in the given band. From extensive ground-based observations, the fluctuation magnitude of bright Virgo ellipticals is known to be $\overline{I} \approx 29.6$ (Tonry et al. 2001). This value must be transformed to the bandpasses of ACS Virgo Cluster Survey, bearing in mind that the correction in this case is required for a typical program galaxy rather than a luminous giant. To estimate this correction, we make use of the scaling relation $\overline{I} \propto 4.5(V-I)$ from Tonry et al. (2001), and assume mean fluctuation colors of $\langle \overline{z}_{850} - \overline{I} \rangle = -0.8$ and $\langle \overline{g}_{475} - \overline{z}_{850} \rangle = 4$ based on the models of Blakeslee, Vazdekis & Ajhar (2001). From Equation 3, we then find $\sigma_L^2 \sim 1.2O_{ij}$ and $\sigma_L^2 \sim 42O_{ij}$ for the g and z bandpasses, respectively.

This estimate of the SBF contribution to the variance does not take into account the effect of the PSF, which will reduce its value per pixel. Convolving simulated noise images with the ACS PSF, we found that the variance per pixel should be reduced by factors of 12 and 14 for the g and z bandpasses, respectively. With the galaxy model, O_{ij}, calculated as described in §2.5 below, the final weight image — including Poisson noise, readnoise and the contribution from the SBF — is then

$$W'_{ij} = TH_{ij}(TD_{ij} + I_{ij} + \kappa O_{ij})^{-1} \tag{4}$$

with $\kappa = 0.1$ and 3 for the g and z bandpasses, respectively. We emphasize again that this SBF "noise" behaves in reality as a signal, and by incorporating its contribution in

the weight images, we are effectively increasing the detection threshold in proportional to the SBF signal. To include these weights in the object detection process, the SExtractor parameter `MAP_RMS` was set to $1/\sqrt{W'_{ij}}$.

For some galaxies, internal dust obscuration, generally confined within the core region, significantly affects the surface brightness profiles and poses problems for both object detection and the estimation of the local background. The method used to flag pixels affected by dust will be described in detail in a future paper; very briefly, an optical depth map is created (in the g band, for convenience) as

$$A_{ij,g} = -2.5 \times [\log(D_{ij,g}/D_{ij,z}) - \log C_{ij}]/(1 - A_z/A_g).$$

This expression applies to the case in which the dust is located entirely in the galaxy's foreground; this assumption is almost certainly incorrect, and so $A_{ij,g}$ represents a strict lower limit to the amount of absorption present. In the dust regions, C_{ij}, the ratio of the unextincted count rates in the g and z band, is estimated by linearly interpolating (or extrapolating, if the dust affects the center) the azimutally averaged values of $D_{ij,g}/D_{ij,z}$ observed in the regions immediately surrounding the dust areas. A pixel is then flagged as affected by dust if $A_{ij,g}$ is positive, larger than the local standard deviation in the dust extinction map, and if more than one contiguous pixel is affected. The last two conditions are necessary in order not to flag noise spikes. In the case of galaxies that contain large scale central dust disks, a more conservative approach was followed prior to object detection and determination of the local background, and the entire disk was masked by hand[2]. For both W_{ij} and W'_{ij}, pixels that were determined to have dust are given zero weight. This prevents them from biasing the background determination (discussed in Sec 2.5), creating false object detections, or biasing the fitting of globular cluster surface brightness profiles. For VCC1316 (M87), pixels lying on its jet where also given zero weight.

2.5. Galaxy Models and Object Detection

A two-dimensional model for each program galaxy, O_{ij}, is needed to compute the weight images used to perform object detection. Once this model is in hand, it is possible to subtract the galaxy and perform the detections on a nearly flat background, greatly simplifying the estimation of the background for the detected sources. This is particularly important in the inner regions of the galaxies, where the background can vary dramatically on small spatial scales.

[2]These galaxies are VCC1030, VCC1154, VCC1250 and VCC1535

Galaxies were modeled using the ELLIPROF program described in the SBF survey of Tonry et al. (1997). This software was used to estimate O_{ij} and construct the weight images that include the contribution of the SBF signal (§2.4). A crucial preliminary step in construction of these models is the determination of the background "sky" count rate for each galaxy. Figure 2 shows the measured count rates, in both the F475W and F850LP filters, for the full sample of galaxies. These count rates, $f_{\rm back}$, refer to the modal pixel values (in units of electrons pixel^{-1} second^{-1}) measured at distances of $\approx$ 90–150″. The upturn seen for the 10 brightest galaxies clearly reflects the contribution of the galaxies themselves to the measured backgrounds (*i.e.*, these galaxies have a median effective radius of $\sim 50''$). To estimate the true background for these objects (all of which have similar locations with respect to the ecliptic plane), we use the fact that the background intensity scales with the SUNANGLE parameter, $\Phi_{\rm sun}$, which gives the angle between the Sun and the V1 axis of the telescope. Figure 3 shows the measured background count rates as a function of $\Phi_{\rm sun}$ for the full sample of galaxies. The dashed curve in each panel shows the function

$$f_{\rm back} = a_i e^{b_i(\Phi - c_i)} + d_i \tag{5}$$

where the values of a_i, b_i, c_i and d_i for each filter have been determined directly from the 90 faintest galaxies in the sample. For the 10 brightest galaxies, which are shown as filled squares in Figure 3, we use equation 5 to estimate the true background count rates.

While the ELLIPROF models generally matched the galaxies quite well, there were in some cases large-scale residuals which remained after subtracting the models. To remove these residuals, the following procedure was adopted. First, SExtractor was run on the image, Δ_{ij}, constructed by subtracting from the science image the galaxy model, *i.e.*, $\Delta_{ij} = D_{ij} - O_{ij}$. The SExtractor image is controlled by the parameters `BACK_FILTERSIZE` and `BACK_SIZE` which, after some experimentation, were set to 1 and 40, respectively.[3] The choice for the latter parameter is particularly important since it must be set to a value small enough to remove much of the structure not accounted for by O_{ij}, yet at the same time large enough to leave the power spectrum of the point spread function (PSF) unaffected. The adopted value of `BACK_SIZE` = 40 accounts for structure on scales of $\gtrsim 2''$ and yet is ≈ 20 times the FWHM of the PSF.

For seven of the galaxies, ELLIPROF was unable to produce acceptable models because of the presence of strong disk components which were not well approximated by elliptical isophotes modulated by low-order Fourier terms.[4] We experimented with parametric

[3]See Bertin & Arnouts (1996) for a discussion of how the background is estimated by SExtractor.

[4]These galaxies are VCC685, VCC1125, VCC1242, VCC1535, VCC1692, VCC1857 and VCC2095.

bulge+disk models, but these also resulted in unacceptably large residuals. Instead, we settled on the same basic approach as used in the ground-based SBF survey for modeling early-type disk galaxies: fitting 2-D bicubic splines after first taking the logarithm of the galaxy image, except here used SExtractor to do the fitting. The logarithmic transformation reduces the steep surface brightness gradients, allowing them to be fitted more accurately by the spline interpolation. We then took the inverse logarithm of the model, subtracted it from the original image, and proceeded with fitting the residuals in linear space as described above.

Object detection on the final subtracted image was performed using a detection threshold of five connected pixels at a 1.5σ significance level. The detections in both the F475W and F850LP images were then matched using a matching radius of $0\farcs1$ which, after some experimentation, was deemed to be optimal: *i.e.*, larger values produced an excess of spurious matches, while some clear associations were missed for smaller choices. A mask was constructed by assigning zero weight to the elliptical regions of the object shape determined by SExtractor and then scaling the a, b parameters by 1.2 times the Kron radius (in units of a). As the Kron radius will include $\sim 94\%$ of the object's flux, the factor of 1.2 ensures that most of the object's flux will be masked. With this object mask, an improved background image, δ_{ij}, is then determined with SExtractor. By masking the objects when estimating δ_{ij}, we avoid biasing of the background by the sources — an important consideration given the rather small value adopted for the `BACK_SIZE` parameter.

The final F475W and F850LP images for object detection, photometry, and SBF analysis are then $F_{ij} = \Delta_{ij} - \delta_{ij}$. Object detection was performed one last time by running SExtractor on F_{ij}, with the detection performed independently in both images, using a detection threshold of five connected pixels at a 1.5σ significance level. Since the background has already been subtracted from F_{ij}, SExtractor was run without further determination of the background (*i.e.*, the background was fixed at a constant value of zero).

The pixel positions of the detections were converted to celestial coordinates using the header information, and those sources detected in a single filter only were discarded. The detections in the F475W and F850LP images were again matched using a matching radius of $0\farcs1$. To investigate the accuracy of the absolute pointing, we compared the coordinates for 950 astrometric standards in our survey fields to those listed in the Guide Star Catalog 2.2 (McLean et al. 1998). We find mean offsets of $-0\farcs20$ and $0\farcs18$ in right ascension and declination, with rms scatter about these value of $0\farcs57$ and $0\farcs70$, respectively. These results are consistent with the absolute pointing accuracy of $\approx 0\farcs3$ reported in Jordán et al. (2004; hereafter Paper III) based upon a comparison of the celestial coordinates of the nucleus of VCC1316 (M87 = NGC4486) with that measured using VLBI. The internal accuracy of the

celestial coordinates for a given galaxy is $\approx 0\farcs01$ (Meurer et al. 2002).

2.6. Globular Cluster Selection, Photometry and Structural Parameters

Our final matched catalog of SExtractor sources consists of globular clusters associated with each galaxy, as well as foreground stars and compact background galaxies. Additional selection criteria were applied to isolate candidate globular clusters for further analysis.

(1) Selection on Magnitude: It is well established that the luminosity function of globular clusters has a near Gaussian form (*e.g.*, Harris 2001). At the distance of Virgo, the luminosity function peaks at $V \approx 23.8$ (Whitmore et al. 1995; Ferrarese, Côté & Jordán 2003). To select a sample of probable globular clusters, we discard all sources in the SExtractor catalog with $g_{475} \leq 19.1$ or $z_{850} \leq 18.0$. These limits are roughly five magnitudes brighter than the expected turnover of the globular cluster luminosity function at the distance of Virgo. For a luminosity function dispersion of $\sigma = 1.40 \pm 0.05$ (Harris 2001), this selection will eliminate $\lesssim 0.02\%$ of the globular clusters associated with the program galaxies, or only ~ 2 clusters from the full survey. In any event, all sources brighter than these cutoffs were inspected visually to identify potentially interesting objects. Figure 4 shows the luminosity distribution of all sources in the SExtractor object catalog for VCC1226 (M49 = NGC4472). The dashed vertical lines in each panel indicate the magnitude cutoff used to select probable globular clusters.

(2) Selection on Shape: Globular clusters in the Local Group are nearly spherical systems, or at most, only modestly flattened. We therefore discard those sources in the SExtractor source catalog which have a mean elongation, $\epsilon \equiv a/b$, measured in the F475W and F850LP filters to be $\langle\epsilon\rangle \geq 2$. This generous limit easily includes even the most elongated clusters in the Milky Way, M31 and the Magellanic Clouds (White & Shawl 1987; Lupton 1989; van den Bergh & Morbey 1994). The distribution of elongations for the full sample of sources in VCC1226 is shown in Figure 5. The inset to this figure compares the elongations measured in the two bandpasses.

In addition to these cuts, any sources found within 10 pixels ($0\farcs5$) of the galaxy centers were omitted from the analysis of the two-dimensional surface brightness profiles of the detected sources (see below). In practice, this criterion eliminates only the nuclei of the program galaxies. The properties of these nuclei, and their relationship to the host galaxies, will be investigated separately in a future paper.

At a distance of ≈ 17 Mpc (Tonry et al. 2001), the globular clusters associated with Virgo galaxies are marginally resolved with WFC/ACS. For example, the mean half-light radius of globular clusters in the Milky Way is $\langle r_h \rangle \approx 3$ pc. This translates into a half-light diameter of $0\farcs07$, or 1.45 pixels — readily measurable given the $\approx 0\farcs1$ FWHM of the PSF in WFC mode.

A Perl/PDL code (KINGPHOT) has been developed (Jordán & Côté 2004) to measure photometric and structural parameters for those sources which satisfied the above criteria by fitting the two-dimensional ACS surface brightness profiles with PSF-convolved isotropic, single-mass King (1966) models. This family of models is well known to provide an excellent representation of the surface brightness profiles of Galactic globular clusters. Empirical PSFs in both F475W and F850LP, varying quadratically with CCD position, were derived using DAOPHOT II (Stetson 1987; 1993) and archival observations of moderately crowded fields in the outskirts of the Galactic globular cluster 47 Tucanae (NGC 104). The observations consisted of a 30 sec F475W image from program GO-9656, and two 60 sec F850LP images from program GO-9018. The archival images were drizzled in the same manner as the science images and a total of ≈ 200 stars were used in each case to determine the PSF.

For each object classified as a globular cluster candidate, KINGPHOT is used to measure the total magnitude, King concentration index, c, and half-light radius, r_h in both bandpasses. Note that we use r_h as scale factor in lieu of the more traditional core radius, r_c, but the two parameters are related as described in McLaughlin (2000). While the selection on magnitude and elongation described above serves to lessen the contamination of the globular cluster catalogs by stars and galaxies, some interlopers inevitably remain. In a future paper, we describe a method to further reduce this contamination for each program galaxy by using our reduction pipeline to analyze archival F475W and F850LP blank field images at high Galactic latitude.

Figures 6 – 8 illustrate the reduction procedures described above for a representative sample of three program galaxies: VCC1226, VCC1422 and VCC1661. These are the first, 50th and 100th ranked galaxies in the survey, respectively. In each figure, we show the registered, geometrically corrected F475W image in the upper left panel. The upper right panel shows the residuals obtained after subtracting from this image the ELLIPROF model described in §2.5. The lower left panel shows the result of subtracting the SExtractor model for this residual background; the circles in this panel indicate those sources which satisfy the criteria used to select globular cluster candidates. Note that bright nuclei of VCC1422 and and VCC1661 are excluded from the respective globular cluster catalogs for these galaxies. The lower right panel shows the image obtained by subtracting the best-fit, PSF-convolved King model from each of the sources identified in the previous panel.

2.7. Foreground Extinction and Photometric Calibration

Since the Virgo Cluster spans $\approx 10^\circ$ on the sky, a reddening for each galaxy was computed using the DIRBE maps of Schlegel, Finkbeiner & Davis (1998). The mean reddening for the sample was found to be $E(B-V) = 0.029$ mag, with a standard deviation of 0.008 mag. The corrections for foreground extinction, assumed to be constant within each ACS field, were taken to be

$$A_g = 3.634E(B-V)$$

$$A_z = 1.485E(B-V).$$

These extinction ratios correspond to the spectral energy distribution of a G2 star (see Table 27 of Sirianni et al. 2004), and are appropriate for the globular clusters and elliptical galaxies targeted in the survey. Calibrated magnitudes on the AB system were obtained using the relations

$$g_{475} = -2.5\log(f_{475}) + 26.068$$

$$z_{850} = -2.5\log(f_{850}) + 24.862$$

where f_{475} and f_{850} refer to the integrated fluxes, in units of electrons/sec, in the F475W and F850LP filters. The photometric zeropoints were taken from Sirianni et al. (2004).

3. Data Products

The reduction pipeline described above was designed to meet the scientific objectives of the ACS Virgo Cluster Survey. Future papers in this series will present scientific results from the survey as well as a variety of data products. These products include a catalog of probable globular clusters associated with each program galaxy and their basic properties (*e.g.*, celestial coordinates, magnitudes, colors and structural parameters) and the results of an isophotal analysis for each galaxy (*e.g*, radial profiles of surface brightness, color, ellipticity, position angle, as well as extinction maps and dust masses). These data products, along with raw and fully processed images used in the analysis, will be made available through the project website: http://www.physics.rutgers.edu/∼pcote/acs.

A.J. extends his thanks to the Oxford Astrophysics Department for their hospitality. Support for program GO-9401 was provided through a grant from the Space Telescope Science Institute, which is operated by the Association of Universities for Research in Astronomy, Inc., under NASA contract NAS5-26555. A.J. acknowledges additional financial support provided by the National Science Foundation through a grant from the Association

of Universities for Research in Astronomy, Inc., under NSF cooperative agreement AST-9613615, and by Fundación Andes under project No.C-13442. P.C. acknowledges additional support provided by NASA LTSA grant NAG5-11714. D.M. is supported by NSF grant AST-020631, NASA grant NAG5-9046, and grant HST-AR-09519.01-A from STScI. M.M. acknowledges additional financial support provided by the Sherman M. Fairchild foundation. M.J.W. acknowledges support through NSF grant AST-0205960. This research has made use of the NASA/IPAC Extragalactic Database (NED) which is operated by the Jet Propulsion Laboratory, California Institute of Technology, under contract with the National Aeronautics and Space Administration.

REFERENCES

Bertin, E. & Arnouts, S. 1996, A&AS, 117, 393

Binggeli, B., Sandage, A., & Tammann, G.A., 1985, AJ, 90, 1681

Blakeslee, J.P., Vazdekis, A., & Ajhar, E. 2001, MNRAS, 320, 193

Blakeslee, J.P., Anderson, K.R., Meurer, G.R. & Benítez, N. 2003, in ASP Conf. Ser. 295: Astronomical Data Analysis Software and Systems XII, 257

Côté, P., Blakeslee, J.P., Ferrarese, L., Jordán, A., Mei, S., Merritt, D., Milosavljević, M., Peng, E.W., & West, M.J. 2004, ApJS, in press (Paper I)

Ferrarese, L., Côté, P., & Jordán, A. 2003, ApJ, 599, 1302

Ford, H.C., et al. 1998, Proc. SPIE, 3356, 234

Harris, W.E. 2001, in Star Clusters, Saas-Fee Advanced School 28, ed. L. Labhardt & B. Binggeli (Berlin:Springer), 223

Jordán, A., Côté, P., Ferrarese, L., Blakeslee, J.P., Mei, S., Merritt, D., Milosavljević, M., Peng, E., Tonry, J.L., & West, M.J. 2004, ApJ, in press (Paper III)

Jordán, A., & Côté, P. 2004, in preparation

King, I.R. 1966, AJ, 71, 64

Koekemoer, A.M., Fruchter, A.S., Hook, R.N., & Hack, W. 2002, in The 2002 HST Calibration Workshop, ed. S. Arribas, A. Koekemoer, & B. Whitmore (STScI: Baltimore), p 339.

Lupton, R.H., 1989, AJ, 97, 1350

McLaughlin 2000, ApJ, 539, 618

McLean, B., Hawkins, C., Spagna, A., Lattanzi, M., Lasker, B., Jenkner, H., White, R. 1998, in IAU Symp. 179, New Horizons from Multi-Wavelength Sky Surveys, ed. B.J. McLean, D.A. Golombek, J.J.E. Hayes, & H.E. Payne (Dordrecht: Kluwer), 431

Meurer, G.R., Lindler, D., Blakeslee, J.P., Cox, C., Martel, A.R., Tran, H.D., Bouwens, R.J., Ford, H.C., Clampin, M., Hartig, G.F., Sirianni, M., & de Marchi, G. 2002, in The 2002 HST Calibration Workshop, ed. S. Arribas, A. Koekemoer, & B. Whitmore (STScI: Baltimore), p 65.

Richmond, M.W., Droege, T.F., Gombert, G., Gutzwiller, M., Henden, A.A., Albertson, C., Beser, N., Molhant, N., & Johnson, H. 2000, PASP, 112, 397

Schlegel, D.J., Finkbeiner, D.P., & Davis, M. 1998, ApJ, 500, 525

Sirianni et al. 2004, in preparation

Stetson, P.B. 1987, PASP, 99, 191

Stetson, P.B. 1993, in IAU Colloq. 136, Stellar Photometry: Current Techniques and Future Developments, ed. C. J. Butler & I. Elliot (Cambridge: Cambridge Univ. Press), 291

Tonry, J.L., & Schneider, D.P. 1988, AJ, 96, 807

Tonry, J. L., Blakeslee, J. P., Ajhar, E. A., & Dressler, A., 1997, ApJ, 475, 399

Tonry, J.L., Dressler, A., Blakeslee, J.P., Ajhar, E.A., Fletcher, A.B., Luppino, G.A., Metzger, M.R., & Moore, C.B. 2001, ApJ, 546, 681

White, R.E., & Shawl, S.J. 1987, ApJ, 317, 246

Whitmore, B.C., Sparks, W.B., Lucas, R.A., Macchetto, F.D., & Biretta, J.A. 1995, ApJ, 454, L73

Valdes, F.G., Campusano, L.E., Velasquez, J.D., & Stetson, P.B. 1995, PASP, 107, 1119

Van den Bergh, S., & Morbey, C.L. 1994, ApJ, 283, 598

Table 1. Log of Observations for GO-9401.

ID	VCC	Date	Dataset	UT	Θ (deg)	T (sec)	Filter
1	1226	2003-06-19	j8fs01x5q	06:50:34	114.72	90	F850LP
			j8fs01x6q	06:54:22		560	F850LP
			j8fs01x8q	07:05:58		560	F850LP
			j8fs01xaq	07:18:11		375	F475W
			j8fs01xcq	07:26:42		375	F475W
2	1316	2003-01-19	j8fs02bdq	20:47:35	269.99	90	F850LP
			j8fs02beq	20:51:23		560	F850LP
			j8fs02bgq	21:02:59		560	F850LP
			j8fs02biq	21:15:12		375	F475W
			j8fs02bkq	21:23:43		375	F475W
3	1978	2003-06-17	j8fs03meq	18:02:11	118.60	90	F850LP
			j8fs03mfq	18:05:59		560	F850LP
			j8fs03mhq	18:17:35		560	F850LP
			j8fs03mjq	18:29:48		375	F475W
			j8fs03mlq	18:38:19		375	F475W
4	881	2003-05-18	j8fs04y3q	08:09:39	140.20	90	F850LP
			j8fs04y4q	08:13:27		560	F850LP
			j8fs04y6q	08:25:03		560	F850LP
			j8fs04y8q	08:37:16		375	F475W
			j8fs04yaq	08:45:47		375	F475W
5	798	2003-02-01	j8fs05dbq	21:00:42	276.94	90	F850LP
			j8fs05dcq	21:04:30		560	F850LP
			j8fs05deq	21:16:06		560	F850LP
			j8fs05dgq	21:28:19		375	F475W
			j8fs05diq	21:36:50		375	F475W
6	763	2003-01-21	j8fs06o0q	20:49:42	285.65	90	F850LP
			j8fs06o1q	20:53:30		560	F850LP
			j8fs06o3q	21:05:06		560	F850LP
			j8fs06o5q	21:17:18		375	F475W
			j8fs06o7q	21:25:50		375	F475W
7	731	2003-06-06	j8fs07f7q	13:08:41	130.00	90	F850LP
			j8fs07f8q	13:12:29		560	F850LP
			j8fs07faq	13:24:05		560	F850LP
			j8fs07fcq	13:36:18		375	F475W
			j8fs07feq	13:44:49		375	F475W
8	1535	2003-07-12	j8fs08lnq	10:18:31	109.20	90	F850LP
			j8fs08loq	10:22:19		560	F850LP
			j8fs08lqq	10:33:55		560	F850LP
			j8fs08lsq	10:46:08		375	F475W
			j8fs08luq	10:54:39		375	F475W
9	1903	2003-07-19	j8fs09lhq	07:09:57	106.61	90	F850LP
			j8fs09liq	07:13:45		560	F850LP
			j8fs09lkq	07:25:21		560	F850LP
			j8fs09lmq	07:37:34		375	F475W
			j8fs09loq	07:46:05		375	F475W

Table 1—Continued

ID	VCC	Date	Dataset	UT	Θ (deg)	T (sec)	Filter
10	1632	2003-07-07	j8fs10eeq	10:17:18	110.94	90	F850LP
			j8fs10efq	10:21:06		560	F850LP
			j8fs10ehq	10:32:42		560	F850LP
			j8fs10ejq	10:44:55		375	F475W
			j8fs10elq	10:53:26		375	F475W
11	1231	2003-06-12	j8fs11a8q	14:47:10	116.84	90	F850LP
			j8fs11a9q	14:50:58		560	F850LP
			j8fs11abq	15:02:34		560	F850LP
			j8fs11adq	15:14:47		375	F475W
			j8fs11afq	15:23:18		375	F475W
12	2095	2003-03-21	j8fs12ipq	18:38:38	227.99	90	F850LP
			j8fs12iqq	18:42:26		560	F850LP
			j8fs12isq	18:54:02		560	F850LP
			j8fs12iuq	19:06:15		375	F475W
			j8fs12iwq	19:14:46		375	F475W
13	1154	2003-07-17	j8fs13xmq	03:56:34	108.61	90	F850LP
			j8fs13xnq	04:00:22		560	F850LP
			j8fs13xpq	04:11:58		560	F850LP
			j8fs13xrq	04:24:11		375	F475W
			j8fs13xtq	04:32:42		375	F475W
14	1062	2003-02-09	j8fs14knq	17:56:13	288.99	90	F850LP
			j8fs14koq	18:00:01		560	F850LP
			j8fs14kqq	18:11:37		560	F850LP
			j8fs14ksq	18:23:50		375	F475W
			j8fs14kuq	18:32:21		375	F475W
15	2092	2003-01-20	j8fs15g6q	22:27:38	287.21	90	F850LP
			j8fs15g7q	22:31:26		560	F850LP
			j8fs15g9q	22:43:02		560	F850LP
			j8fs15gbq	22:55:14		375	F475W
			j8fs15gdq	23:03:46		375	F475W
16	369	2003-06-14	j8fs16t2q	19:35:28	129.80	90	F850LP
			j8fs16t3q	19:39:16		560	F850LP
			j8fs16t5q	19:50:52		560	F850LP
			j8fs16t7q	20:03:05		375	F475W
			j8fs16t9q	20:11:36		375	F475W
17	759	2003-06-11	j8fs17pnq	08:22:38	112.81	90	F850LP
			j8fs17poq	08:26:26		560	F850LP
			j8fs17pqq	08:38:02		560	F850LP
			j8fs17psq	08:50:15		375	F475W
			j8fs17puq	08:58:46		375	F475W
18	1692	2003-07-13	j8fs18tnq	07:06:54	109.80	90	F850LP
			j8fs18toq	07:10:42		560	F850LP
			j8fs18tqq	07:22:18		560	F850LP
			j8fs18tsq	07:34:31		375	F475W
			j8fs18tuq	07:43:02		375	F475W

Table 1—Continued

ID	VCC	Date	Dataset	UT	Θ (deg)	T (sec)	Filter
19	1030	2003-01-31	j8fs19ucq	20:59:27	290.19	90	F850LP
			j8fs19udq	21:03:15		560	F850LP
			j8fs19ufq	21:14:51		560	F850LP
			j8fs19uhq	21:27:03		375	F475W
			j8fs19ujq	21:35:35		375	F475W
20	2000	2003-06-21	j8fs20j8q	06:52:14	124.00	90	F850LP
			j8fs20j9q	06:56:02		560	F850LP
			j8fs20jbq	07:07:38		560	F850LP
			j8fs20jdq	07:19:51		375	F475W
			j8fs20jfq	07:28:22		375	F475W
21	685	2003-06-13	j8fs21mcq	17:58:47	116.47	90	F850LP
			j8fs21mdq	18:02:35		560	F850LP
			j8fs21mfq	18:14:11		560	F850LP
			j8fs21mhq	18:26:24		375	F475W
			j8fs21mjq	18:34:55		375	F475W
22	1664	2003-07-07	j8fs22etq	11:54:55	111.15	90	F850LP
			j8fs22euq	11:58:43		560	F850LP
			j8fs22ewq	12:10:19		560	F850LP
			j8fs22eyq	12:22:32		375	F475W
			j8fs22f0q	12:31:03		375	F475W
23	654	2003-06-10	j8fs23mnq	21:09:46	120.01	90	F850LP
			j8fs23moq	21:13:34		560	F850LP
			j8fs23mqq	21:25:10		560	F850LP
			j8fs23msq	21:37:23		375	F475W
			j8fs23muq	21:45:54		375	F475W
24	944	2003-06-12	j8fs24zpq	13:11:28	116.00	90	F850LP
			j8fs24zqq	13:15:16		560	F850LP
			j8fs24zsq	13:26:52		560	F850LP
			j8fs24zuq	13:39:05		375	F475W
			j8fs24zwq	13:47:36		375	F475W
25	1938	2003-03-05	j8fs25cnq	21:30:57	249.98	90	F850LP
			j8fs25coq	21:34:45		560	F850LP
			j8fs25cqq	21:46:21		560	F850LP
			j8fs25csq	21:58:33		375	F475W
			j8fs25cuq	22:07:05		375	F475W
26	1279	2003-07-09	j8fs26tiq	08:41:47	110.32	90	F850LP
			j8fs26tjq	08:45:35		560	F850LP
			j8fs26tlq	08:57:11		560	F850LP
			j8fs26tnq	09:09:24		375	F475W
			j8fs26tpq	09:17:55		375	F475W
27	1720	2003-05-15	j8fs27a9q	08:08:29	129.00	90	F850LP
			j8fs27aaq	08:12:17		560	F850LP
			j8fs27acq	08:23:53		560	F850LP
			j8fs27aeq	08:36:06		375	F475W
			j8fs27agq	08:44:37		375	F475W

Table 1—Continued

ID	VCC	Date	Dataset	UT	Θ (deg)	T (sec)	Filter
28	355	2003-06-13	j8fs28jrq	09:58:40	116.03	90	F850LP
			j8fs28jsq	10:02:28		560	F850LP
			j8fs28juq	10:14:04		560	F850LP
			j8fs28jwq	10:26:17		375	F475W
			j8fs28jyq	10:34:48		375	F475W
29	1619	2003-07-18	j8fs29gcq	08:45:12	110.61	90	F850LP
			j8fs29gdq	08:49:00		560	F850LP
			j8fs29gfq	09:00:36		560	F850LP
			j8fs29ghq	09:12:49		375	F475W
			j8fs29gjq	09:21:20		375	F475W
30	1883	2003-03-19	j8fs30t7q	17:00:03	239.94	90	F850LP
			j8fs30t8q	17:03:51		560	F850LP
			j8fs30taq	17:15:27		560	F850LP
			j8fs30tcq	17:27:40		375	F475W
			j8fs30teq	17:36:11		375	F475W
31	1242	2003-03-20	j8fs31awq	17:00:56	179.98	90	F850LP
			j8fs31axq	17:04:44		560	F850LP
			j8fs31azq	17:16:20		560	F850LP
			j8fs31b1q	17:28:33		375	F475W
			j8fs31b3q	17:37:04		375	F475W
32	784	2003-06-13	j8fs32luq	16:22:59	111.61	90	F850LP
			j8fs32lvq	16:26:47		560	F850LP
			j8fs32lxq	16:38:23		560	F850LP
			j8fs32lzq	16:50:36		375	F475W
			j8fs32m1q	16:59:07		375	F475W
33	1537	2003-01-20	j8fs33flq	19:12:52	286.93	90	F850LP
			j8fs33fmq	19:16:40		560	F850LP
			j8fs33foq	19:28:16		560	F850LP
			j8fs33fqq	19:40:30		375	F475W
			j8fs33fsq	19:49:00		375	F475W
34	778	2003-06-16	j8fs34elq	18:00:11	130.20	90	F850LP
			j8fs34emq	18:03:59		560	F850LP
			j8fs34eoq	18:15:35		560	F850LP
			j8fs34eqq	18:27:48		375	F475W
			j8fs34esq	18:36:19		375	F475W
35	1321	2003-07-16	j8fs35seq	05:32:39	106.93	90	F850LP
			j8fs35sfq	05:36:27		560	F850LP
			j8fs35shq	05:48:03		560	F850LP
			j8fs35sjq	06:00:16		375	F475W
			j8fs35slq	06:08:47		375	F475W
36	828	2003-07-17	j8fs36y3s	05:32:16	106.41	90	F850LP
			j8fs36y4q	05:36:04		560	F850LP
			j8fs36y6q	05:47:40		560	F850LP
			j8fs36y8q	05:59:53		375	F475W
			j8fs36yaq	06:08:24		375	F475W

Table 1—Continued

ID	VCC	Date	Dataset	UT	Θ (deg)	T (sec)	Filter
37	1250	2003-01-20	j8fs37fwq	20:48:46	286.35	90	F850LP
			j8fs37fxq	20:52:34		560	F850LP
			j8fs37fzq	21:04:10		560	F850LP
			j8fs37g1q	21:16:22		375	F475W
			j8fs37g3q	21:24:54		375	F475W
38	1630	2003-07-30	j8fs38s0q	05:39:01	100.01	90	F850LP
			j8fs38s1q	05:42:49		560	F850LP
			j8fs38s3q	05:54:25		560	F850LP
			j8fs38s5q	06:06:38		375	F475W
			j8fs38s7q	06:15:09		375	F475W
39	1146	2003-12-28	j8fs39cbq	22:19:27	285.99	90	F850LP
			j8fs39ccq	22:23:15		560	F850LP
			j8fs39ceq	22:34:51		560	F850LP
			j8fs39cgq	22:47:04		375	F475W
			j8fs39ciq	22:55:35		375	F475W
40	1025	2003-04-05	j8fs40g6q	17:13:05	174.99	90	F850LP
			j8fs40g7q	17:16:53		560	F850LP
			j8fs40g9q	17:28:29		560	F850LP
			j8fs40gbq	17:40:42		375	F475W
			j8fs40gdq	17:49:13		375	F475W
41	1303	2003-07-09	j8fs41txq	10:17:26	114.60	90	F850LP
			j8fs41tyq	10:21:14		560	F850LP
			j8fs41u0q	10:32:50		560	F850LP
			j8fs41u2q	10:45:03		375	F475W
			j8fs41u4q	10:53:34		375	F475W
42	1913	2003-04-28	j8fs42kuq	19:05:58	131.00	90	F850LP
			j8fs42kvq	19:09:46		560	F850LP
			j8fs42kxq	19:21:22		560	F850LP
			j8fs42kzq	19:33:35		375	F475W
			j8fs42l1q	19:42:06		375	F475W
43	1327	2003-06-12	j8fs43aqq	16:23:25	116.61	90	F850LP
			j8fs43arq	16:27:13		560	F850LP
			j8fs43atq	16:38:49		560	F850LP
			j8fs43avq	16:51:02		375	F475W
			j8fs43axq	16:59:33		375	F475W
44	1125	2003-06-11	j8fs44qbq	09:58:52	117.01	90	F850LP
			j8fs44qcq	10:02:40		560	F850LP
			j8fs44qeq	10:14:16		560	F850LP
			j8fs44qgq	10:26:29		375	F475W
			j8fs44qiq	10:35:00		375	F475W
45	1475	2003-06-12	j8fs45b8q	17:59:01	117.21	90	F850LP
			j8fs45b9q	18:02:49		560	F850LP
			j8fs45bbq	18:14:25		560	F850LP
			j8fs45bdq	18:26:38		375	F475W
			j8fs45bfq	18:35:09		375	F475W

Table 1—Continued

ID	VCC	Date	Dataset	UT	Θ (deg)	T (sec)	Filter
46	1178	2003-01-25	j8fs46hjq	20:53:34	287.17	90	F850LP
			j8fs46hkq	20:57:22		560	F850LP
			j8fs46hmq	21:08:58		560	F850LP
			j8fs46hoq	21:21:11		375	F475W
			j8fs46hqq	21:29:42		375	F475W
47	1283	2002-12-25	j8fs47tkq	18:39:12	301.00	90	F850LP
			j8fs47tlq	18:43:00		560	F850LP
			j8fs47tnq	18:54:36		560	F850LP
			j8fs47tpq	19:06:49		375	F475W
			j8fs47trq	19:15:20		375	F475W
48	1261	2003-07-13	j8fs48u4q	08:42:58	111.61	90	F850LP
			j8fs48u5q	08:46:46		560	F850LP
			j8fs48u7q	08:58:22		560	F850LP
			j8fs48u9q	09:10:35		375	F475W
			j8fs48ubq	09:19:06		375	F475W
49	698	2003-06-21	j8fs49jpq	08:26:52	128.00	90	F850LP
			j8fs49jqq	08:30:40		560	F850LP
			j8fs49jsq	08:42:16		560	F850LP
			j8fs49juq	08:54:29		375	F475W
			j8fs49jwq	09:03:00		375	F475W
50	1422	2003-07-09	j8fs50ueq	11:55:43	112.21	90	F850LP
			j8fs50ufq	11:59:31		560	F850LP
			j8fs50uhq	12:11:07		560	F850LP
			j8fs50ujq	12:23:20		375	F475W
			j8fs50ulq	12:31:51		375	F475W
51	2048	2003-06-08	j8fs51tsq	14:46:55	131.80	90	F850LP
			j8fs51ttq	14:50:43		560	F850LP
			j8fs51tvq	15:02:19		560	F850LP
			j8fs51txq	15:14:32		375	F475W
			j8fs51tzq	15:23:03		375	F475W
52	1871	2003-07-11	j8fs52epq	07:07:02	111.41	90	F850LP
			j8fs52eqq	07:10:50		560	F850LP
			j8fs52esq	07:22:26		560	F850LP
			j8fs52euq	07:34:39		375	F475W
			j8fs52ewq	07:43:10		375	F475W
53	9	2003-01-21	j8fs53n9q	19:12:36	265.78	90	F850LP
			j8fs53naq	19:16:24		560	F850LP
			j8fs53ncq	19:28:00		560	F850LP
			j8fs53neq	19:40:14		375	F475W
			j8fs53ngq	19:48:44		375	F475W
54	575	2003-07-13	j8fs54ulq	10:18:14	110.61	90	F850LP
			j8fs54umq	10:22:02		560	F850LP
			j8fs54uoq	10:33:38		560	F850LP
			j8fs54uqq	10:45:51		375	F475W
			j8fs54usq	10:54:22		375	F475W

Table 1—Continued

ID	VCC	Date	Dataset	UT	Θ (deg)	T (sec)	Filter
55	1910	2003-01-31	j8fs55t3q	17:48:02	283.02	90	F850LP
			j8fs55t4q	17:51:50		560	F850LP
			j8fs55t6q	18:03:26		560	F850LP
			j8fs55t8q	18:15:39		375	F475W
			j8fs55taq	18:24:10		375	F475W
56	1049	2003-02-12	j8fs56t5q	14:47:23	289.99	90	F850LP
			j8fs56t6q	14:51:11		560	F850LP
			j8fs56t8q	15:02:47		560	F850LP
			j8fs56taq	15:15:00		375	F475W
			j8fs56tcq	15:23:31		375	F475W
57	856	2003-07-11	j8fs57f8q	08:41:59	109.21	90	F850LP
			j8fs57f9q	08:45:47		560	F850LP
			j8fs57fbq	08:57:23		560	F850LP
			j8fs57fdq	09:09:36		375	F475W
			j8fs57ffq	09:18:07		375	F475W
58	140	2003-06-15	j8fs58beq	09:59:11	115.61	90	F850LP
			j8fs58bfq	10:02:59		560	F850LP
			j8fs58bhq	10:14:35		560	F850LP
			j8fs58bjq	10:26:48		375	F475W
			j8fs58blq	10:35:19		375	F475W
59	1355	2003-01-21	j8fs59kcq	16:01:59	285.20	90	F850LP
			j8fs59kdq	16:05:47		560	F850LP
			j8fs59kfq	16:17:23		560	F850LP
			j8fs59khq	16:29:36		375	F475W
			j8fs59kjq	16:38:07		375	F475W
60	1087	2003-01-31	j8fs60txq	19:23:16	280.79	90	F850LP
			j8fs60tyq	19:27:04		560	F850LP
			j8fs60u0q	19:38:40		560	F850LP
			j8fs60u2q	19:50:53		375	F475W
			j8fs60u4q	19:59:24		375	F475W
61	1297	2003-02-25	j8fs61n8q	14:58:09	243.38	90	F850LP
			j8fs61n9q	15:01:57		560	F850LP
			j8fs61nbq	15:13:33		560	F850LP
			j8fs61ndq	15:25:46		375	F475W
			j8fs61nfq	15:34:17		375	F475W
62	1861	2003-11-20	j8fs62lbq	23:52:41	300.80	90	F850LP
			j8fs62lcq	23:56:29		560	F850LP
		2003-11-21	j8fs62leq	00:08:05		560	F850LP
			j8fs62lgq	00:20:18		375	F475W
			j8fs62liq	00:28:49		375	F475W
63	543	2003-02-25	j8fs63mrq	13:21:25	249.98	90	F850LP
			j8fs63msq	13:25:13		560	F850LP
			j8fs63muq	13:36:49		560	F850LP
			j8fs63mwq	13:49:02		375	F475W
			j8fs63myq	13:57:33		375	F475W

Table 1—Continued

ID	VCC	Date	Dataset	UT	Θ (deg)	T (sec)	Filter
64	1431	2003-01-10	j8fs64ccq	23:45:46	300.00	90	F850LP
			j8fs64cdq	23:49:34		560	F850LP
		2003-01-11	j8fs64cfq	00:01:10		560	F850LP
			j8fs64chq	00:13:22		375	F475W
			j8fs64cjq	00:21:54		375	F475W
65	1528	2003-01-22	j8fs65whq	19:15:22	285.27	90	F850LP
			j8fs65wiq	19:19:10		560	F850LP
			j8fs65wkq	19:30:46		560	F850LP
			j8fs65wmq	19:42:59		375	F475W
			j8fs65woq	19:51:30		375	F475W
66	1695	2003-02-01	j8fs66clq	19:24:47	281.96	90	F850LP
			j8fs66cmq	19:28:35		560	F850LP
			j8fs66coq	19:40:11		560	F850LP
			j8fs66cqq	19:52:24		375	F475W
			j8fs66csq	20:00:55		375	F475W
67	1833	2003-03-20	j8fs67baq	18:37:57	213.63	90	F850LP
			j8fs67bbq	18:41:45		560	F850LP
			j8fs67bdq	18:53:21		560	F850LP
			j8fs67bfq	19:05:34		375	F475W
			j8fs67bhq	19:14:05		375	F475W
68	437	2003-07-15	j8fs68mhq	10:19:56	106.81	90	F850LP
			j8fs68miq	10:23:44		560	F850LP
			j8fs68mkq	10:35:20		560	F850LP
			j8fs68mmq	10:47:33		375	F475W
			j8fs68moq	10:56:04		375	F475W
69	2019	2003-03-19	j8fs69tnq	18:37:08	224.18	90	F850LP
			j8fs69toq	18:40:56		560	F850LP
			j8fs69tqq	18:52:33		560	F850LP
			j8fs69tsq	19:04:46		375	F475W
			j8fs69tuq	19:13:17		375	F475W
70	33	2003-07-15	j8fs70l0q	05:30:55	107.56	90	F850LP
			j8fs70l1q	05:34:43		560	F850LP
			j8fs70l3q	05:46:19		560	F850LP
			j8fs70l5q	05:58:32		375	F475W
			j8fs70l7q	06:07:03		375	F475W
71	200	2003-06-11	j8fs71qxq	11:34:02	115.21	90	F850LP
			j8fs71qyq	11:37:50		560	F850LP
			j8fs71r0q	11:49:26		560	F850LP
			j8fs71r2q	12:01:39		375	F475W
			j8fs71r4q	12:10:10		375	F475W
72	571	2003-06-23	j8fs72d0q	11:40:35	119.80	90	F850LP
			j8fs72d1q	11:44:23		560	F850LP
			j8fs72d3q	11:55:59		560	F850LP
			j8fs72d5q	12:08:12		375	F475W
			j8fs72d7q	12:16:43		375	F475W

Table 1—Continued

ID	VCC	Date	Dataset	UT	Θ (deg)	T (sec)	Filter
73	21	2003-05-20	j8fs73nrq	14:34:15	131.80	90	F850LP
			j8fs73nsq	14:38:03		560	F850LP
			j8fs73nuq	14:49:39		560	F850LP
			j8fs73nwq	15:01:52		375	F475W
			j8fs73nyq	15:10:23		375	F475W
74	1488	2003-07-13	j8fs74x8q	19:55:08	113.01	90	F850LP
			j8fs74x9q	19:58:56		560	F850LP
			j8fs74xbq	20:10:32		560	F850LP
			j8fs74xdq	20:22:45		375	F475W
			j8fs74xfq	20:31:16		375	F475W
75	1779	2003-07-19	j8fs75lwq	08:46:03	104.01	90	F850LP
			j8fs75lxq	08:49:51		560	F850LP
			j8fs75lzq	09:01:27		560	F850LP
			j8fs75m1q	09:13:40		375	F475W
			j8fs75m3q	09:22:11		375	F475W
76	1895	2003-07-12	j8fs76m2q	11:57:17	108.01	90	F850LP
			j8fs76m3q	12:01:05		560	F850LP
			j8fs76m5q	12:12:41		560	F850LP
			j8fs76m7q	12:24:54		375	F475W
			j8fs76m9q	12:33:25		375	F475W
77	1499	2003-07-14	j8fs77b4q	03:55:42	110.21	90	F850LP
			j8fs77b5q	03:59:30		560	F850LP
			j8fs77b7q	04:11:06		560	F850LP
			j8fs77b9q	04:23:19		375	F475W
			j8fs77bbq	04:31:50		375	F475W
78	1545	2003-07-14	j8fs78ccq	05:31:40	110.61	90	F850LP
			j8fs78cdq	05:35:28		560	F850LP
			j8fs78cfq	05:47:04		560	F850LP
			j8fs78chq	05:59:17		375	F475W
			j8fs78cjq	06:07:48		375	F475W
79	1192	2003-06-06	j8fs79fwq	14:45:00	130.00	90	F850LP
			j8fs79fxq	14:48:48		560	F850LP
			j8fs79fzq	15:00:24		560	F850LP
			j8fs79g1q	15:12:37		375	F475W
			j8fs79g3q	15:21:08		375	F475W
80	1857	2003-04-17	j8fs80lhq	10:58:12	148.00	90	F850LP
			j8fs80liq	11:02:00		560	F850LP
			j8fs80lkq	11:13:36		560	F850LP
			j8fs80lmq	11:25:49		375	F475W
			j8fs80loq	11:34:20		375	F475W
81	1075	2003-07-14	j8fs81cxq	07:07:09	106.61	90	F850LP
			j8fs81cyq	07:10:57		560	F850LP
			j8fs81d0q	07:22:33		560	F850LP
			j8fs81d2q	07:34:46		375	F475W
			j8fs81d4q	07:43:17		375	F475W

Table 1—Continued

ID	VCC	Date	Dataset	UT	Θ (deg)	T (sec)	Filter
82	1948	2003-07-14	j8fs82deq	08:44:04	112.21	90	F850LP
			j8fs82dfq	08:47:52		560	F850LP
			j8fs82dhq	08:59:28		560	F850LP
			j8fs82djq	09:11:41		375	F475W
			j8fs82dlq	09:20:12		375	F475W
83	1627	2003-01-22	j8fs83wzq	20:51:27	285.77	90	F850LP
			j8fs83x0q	20:55:15		560	F850LP
			j8fs83x2q	21:06:51		560	F850LP
			j8fs83x4q	21:19:04		375	F475W
			j8fs83x6q	21:27:35		375	F475W
84	1440	2003-07-13	j8fs84v0q	11:57:56	108.38	90	F850LP
			j8fs84v1q	12:01:44		560	F850LP
			j8fs84v3q	12:13:20		560	F850LP
			j8fs84v5q	12:25:33		375	F475W
			j8fs84v7q	12:34:04		375	F475W
85	230	2003-07-15	j8fs85llq	07:07:01	107.41	90	F850LP
			j8fs85lmq	07:10:49		560	F850LP
			j8fs85loq	07:22:25		560	F850LP
			j8fs85lqq	07:34:38		375	F475W
			j8fs85lsq	07:43:09		375	F475W
86	2050	2003-03-23	j8fs86v1q	17:03:34	220.38	90	F850LP
			j8fs86v2q	17:07:22		560	F850LP
			j8fs86v4q	17:18:58		560	F850LP
			j8fs86v6q	17:31:11		375	F475W
			j8fs86v8q	17:39:42		375	F475W
87	1993	2003-01-31	j8fs87rcq	14:36:10	282.30	90	F850LP
			j8fs87rdq	14:39:58		560	F850LP
			j8fs87rfq	14:51:34		560	F850LP
			j8fs87rhq	15:03:47		375	F475W
			j8fs87rjq	15:12:18		375	F475W
88	751	2003-06-19	j8fs88xjq	08:24:44	120.01	90	F850LP
			j8fs88xks	08:28:32		560	F850LP
			j8fs88xmq	08:40:08		560	F850LP
			j8fs88xoq	08:52:21		375	F475W
			j8fs88xqq	09:00:52		375	F475W
89	1828	2003-01-31	j8fs89scq	16:11:59	282.24	90	F850LP
			j8fs89sdq	16:15:47		560	F850LP
			j8fs89sfq	16:27:23		560	F850LP
			j8fs89shq	16:39:36		375	F475W
			j8fs89sjq	16:48:07		375	F475W
90	538	2003-07-14	j8fs90dvq	10:18:27	110.20	90	F850LP
			j8fs90dwq	10:22:15		560	F850LP
			j8fs90dyq	10:33:51		560	F850LP
			j8fs90e0q	10:46:04		375	F475W
			j8fs90e2q	10:54:35		375	F475W

Table 1—Continued

ID	VCC	Date	Dataset	UT	Θ (deg)	T (sec)	Filter
91	1407	2003-07-15	j8fs91jgq	02:19:49	110.81	90	F850LP
			j8fs91jhq	02:23:37		560	F850LP
			j8fs91jjq	02:35:13		560	F850LP
			j8fs91jlq	02:47:26		375	F475W
			j8fs91jnq	02:55:57		375	F475W
92	1886	2003-07-15	j8fs92klq	03:56:27	110.81	90	F850LP
			j8fs92kmq	04:00:15		560	F850LP
			j8fs92koq	04:11:51		560	F850LP
			j8fs92kqq	04:24:04		375	F475W
			j8fs92ksq	04:32:35		375	F475W
93	1199	2003-02-24	j8fs93i3q	22:58:17	253.79	90	F850LP
			j8fs93i4q	23:02:05		560	F850LP
			j8fs93i6q	23:13:41		560	F850LP
			j8fs93i8q	23:25:54		375	F475W
			j8fs93iaq	23:34:25		375	F475W
94	1743	2003-07-18	j8fs94grq	10:21:12	107.41	90	F850LP
			j8fs94gsq	10:25:00		560	F850LP
			j8fs94guq	10:36:36		560	F850LP
			j8fs94gwq	10:48:49		375	F475W
			j8fs94gyq	10:57:20		375	F475W
95	1539	2003-06-24	j8fs95jgq	08:29:37	113.81	90	F850LP
			j8fs95jhq	08:33:25		560	F850LP
			j8fs95jjq	08:45:01		560	F850LP
			j8fs95jlq	08:57:14		375	F475W
			j8fs95jnq	09:05:45		375	F475W
96	1185	2003-07-11	j8fs96fnq	10:18:30	114.21	90	F850LP
			j8fs96foq	10:22:18		560	F850LP
			j8fs96fqq	10:33:54		560	F850LP
			j8fs96fsq	10:46:07		375	F475W
			j8fs96fuq	10:54:38		375	F475W
97	1826	2003-01-21	j8fs97lrq	17:38:15	278.39	90	F850LP
			j8fs97lsq	17:42:03		560	F850LP
			j8fs97luq	17:53:39		560	F850LP
			j8fs97lwq	18:05:52		375	F475W
			j8fs97lyq	18:14:23		375	F475W
98	1512	2003-07-19	j8fs98kxq	05:33:22	106.21	90	F850LP
			j8fs98kyq	05:37:10		560	F850LP
			j8fs98l0q	05:48:46		560	F850LP
			j8fs98l2q	06:00:59		375	F475W
			j8fs98l4q	06:09:30		375	F475W
99	1489	2003-07-15	j8fs99m2q	08:43:52	111.61	90	F850LP
			j8fs99m3q	08:47:40		560	F850LP
			j8fs99m5q	08:59:16		560	F850LP
			j8fs99m7q	09:11:29		375	F475W
			j8fs99m9q	09:20:00		375	F475W

Table 1—Continued

ID	VCC	Date	Dataset	UT	Θ (deg)	T (sec)	Filter
100	1661	2003-12-25	j8fsa0f4q	23:56:43	289.99	90	F850LP
		2003-12-26	j8fsa0f5q	00:00:31		560	F850LP
			j8fsa0f7q	00:12:07		560	F850LP
			j8fsa0f9q	00:24:20		375	F475W
			j8fsa0fbq	00:32:51		375	F475W

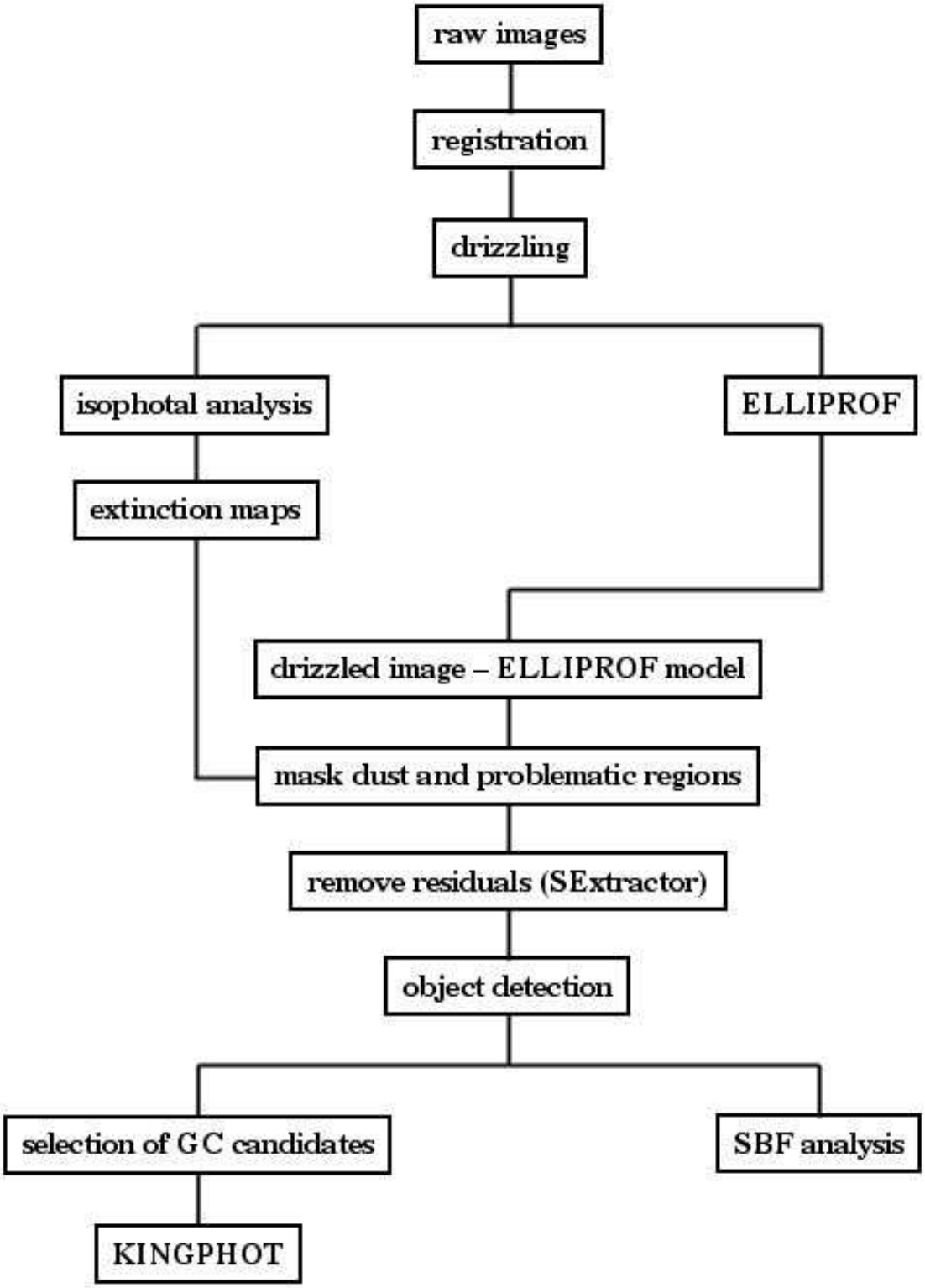

Fig. 1.— Schematic representation of the data reduction pipeline for the ACS Virgo Cluster Survey.

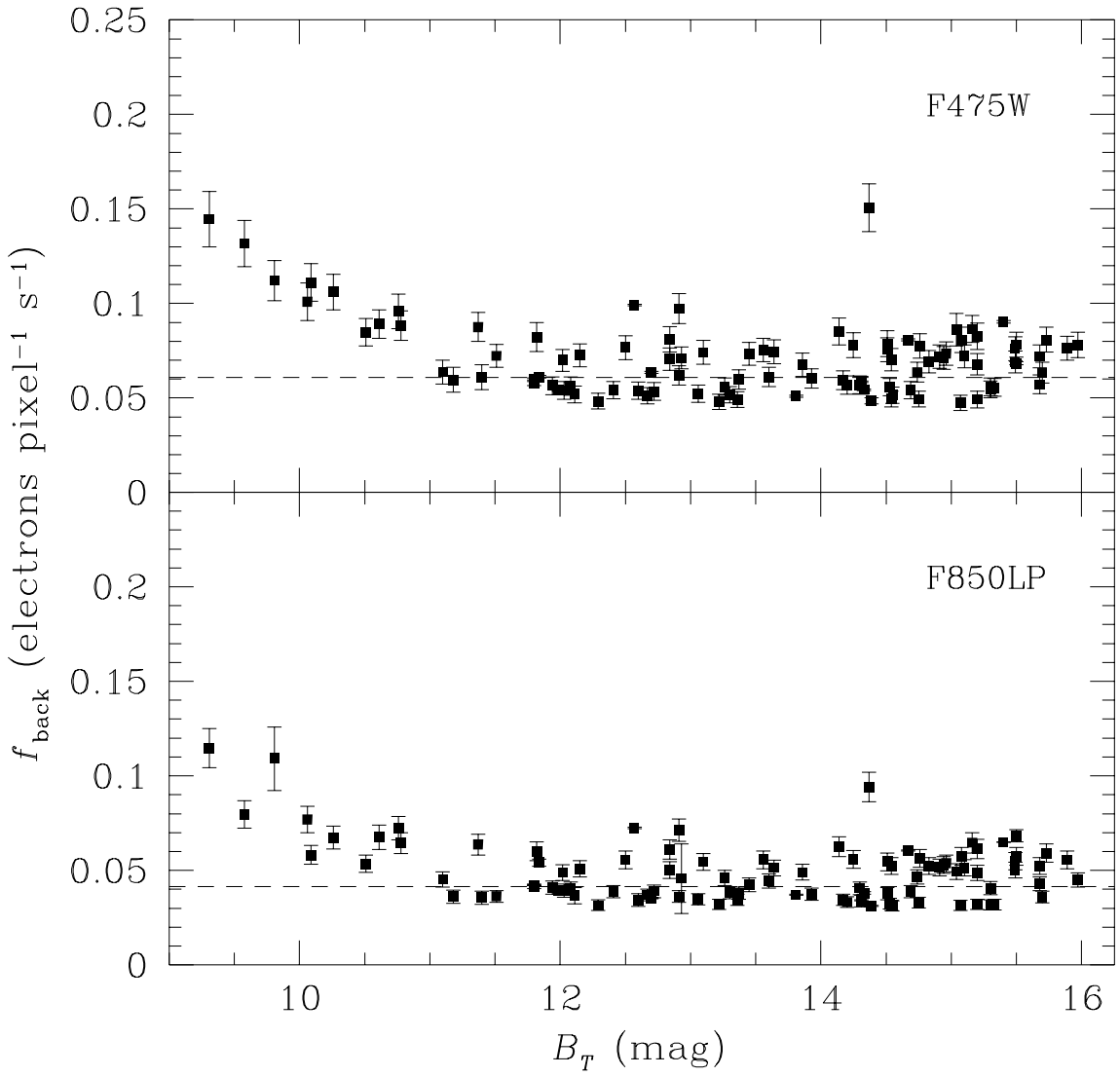

Fig. 2.— Background count rates measured at $R \gtrsim 90''$ in the F475W and F850LP (upper and lower panels, respectively). The dashed lines in upper and lower panels show the count rates reported in the ACS Instrument Handbook: $f_{\rm back} = 0.0609$ and 0.0415 electrons pixel^{-1} second^{-1}, respectively.

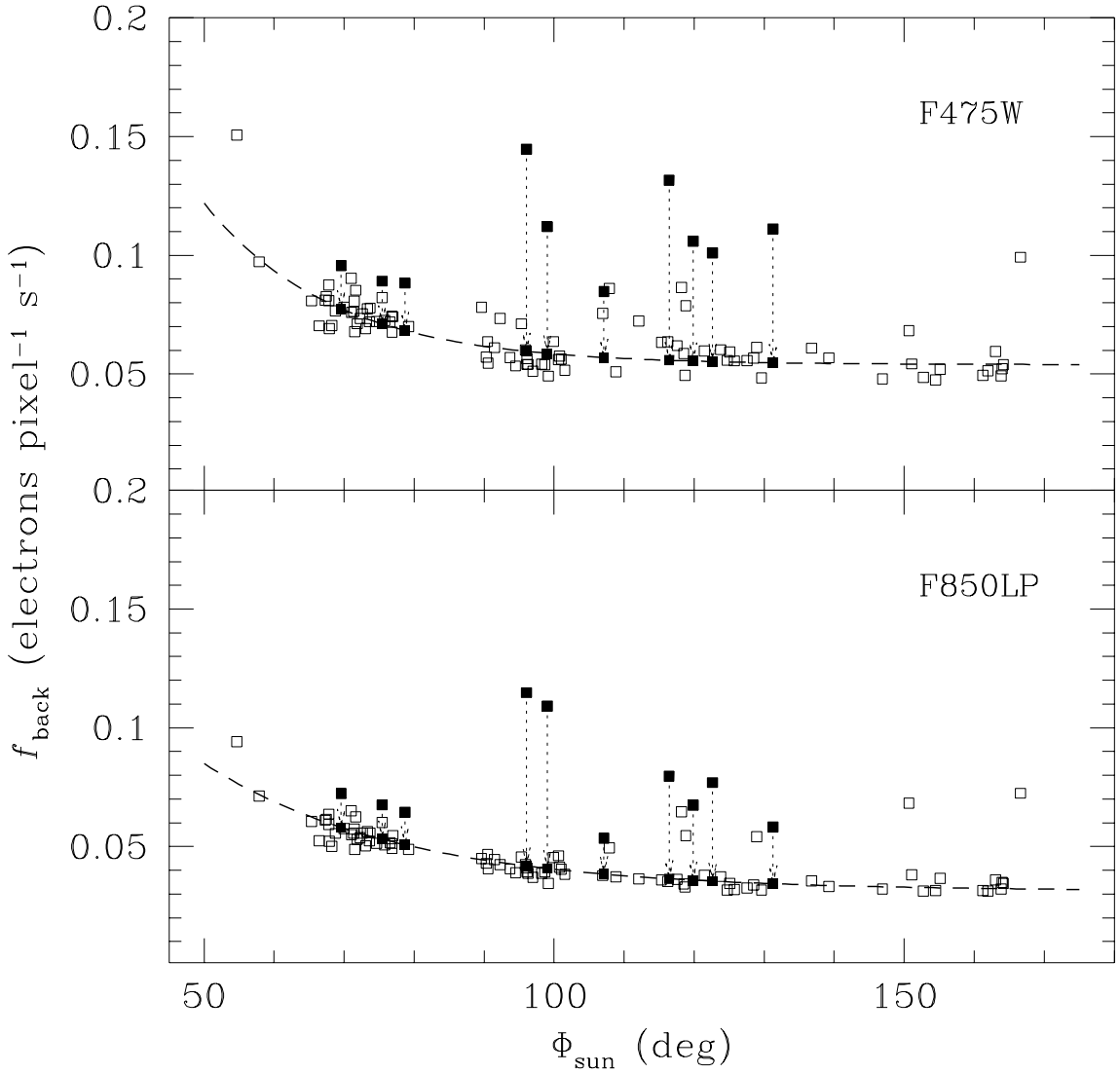

Fig. 3.— Background count rates in F475W (upper panel) and F850LP (lower panel) plotted as a function of $\Phi_{\rm sun}$. The dashed curve in each panel shows a parametric representation of the form of equation 5, determined directly from the 90 faintest galaxies in the sample. The measured count rates for the 10 brightest galaxies are shown by the upper filled squares; the adopted values are indicated by the lower filled squares.

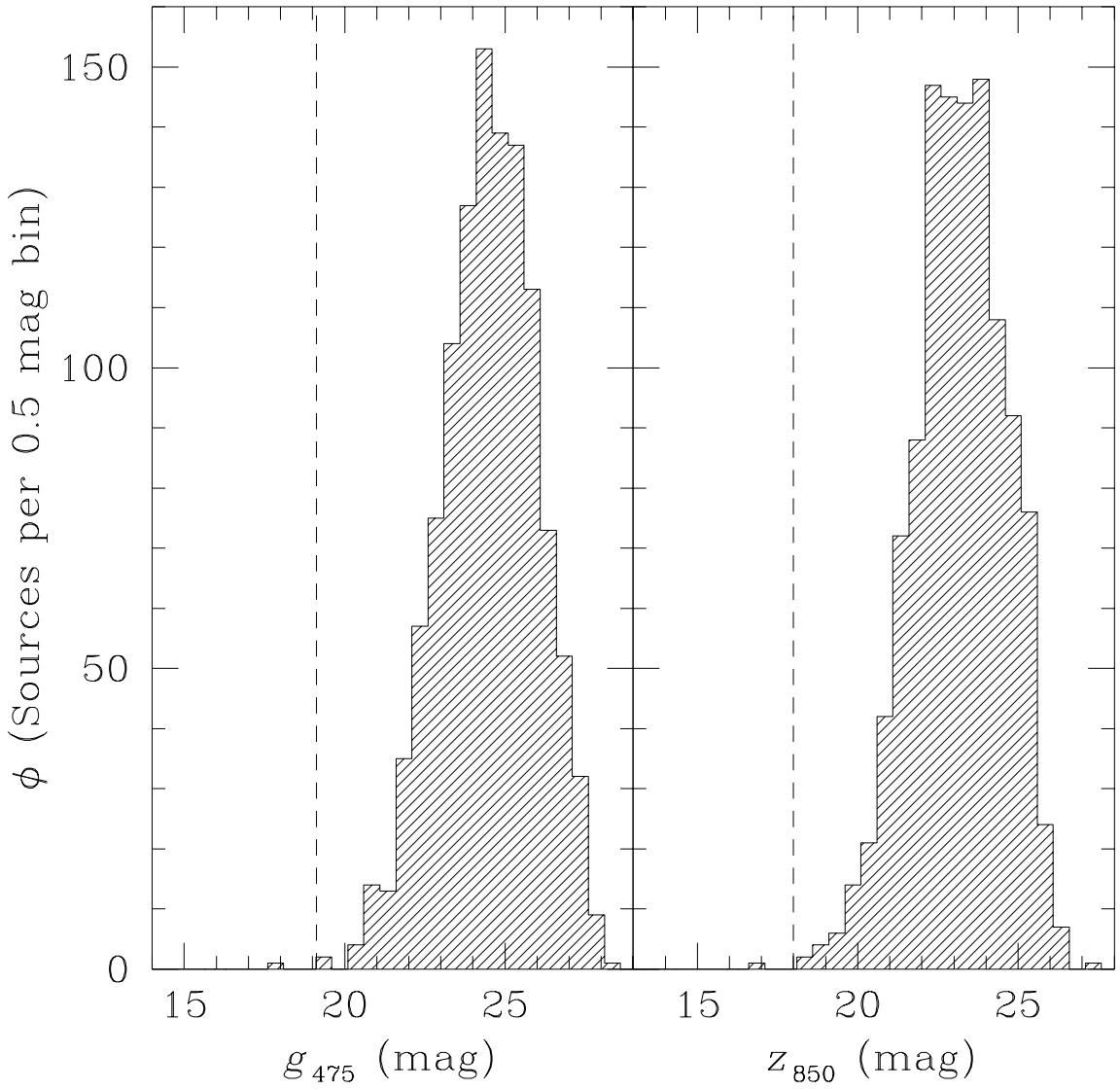

Fig. 4.— *(Left Panel)* Luminosity function, ϕ, in g_{475} for all 1144 sources detected in VCC1226 (M49 = NGC4472). The vertical dashed line indicates the magnitude selection used to identify probable globular clusters. *(Right Panel)* Same as the previous panel, except for z_{850}.

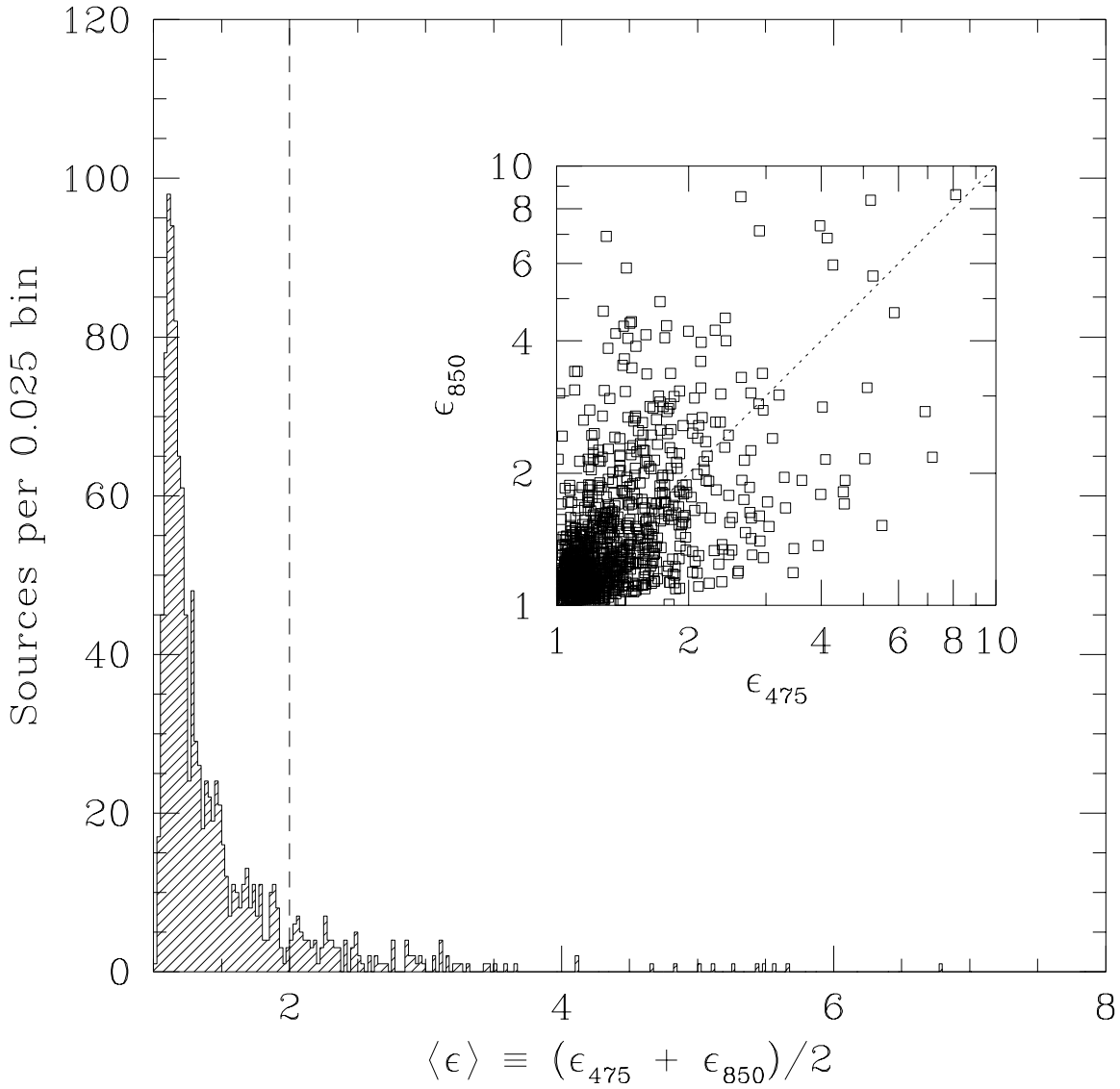

Fig. 5.— Distribution of mean elongations, $\langle\epsilon\rangle$, for all 1144 sources detected in the field of VCC1226 (M49 = NGC4472). The vertical dashed line indicates the selection on elongation, $\langle\epsilon\rangle < 2$, used to identify probable globular clusters. *(Inset)* Comparison of the elongations measured in the F475W and F850LP images.

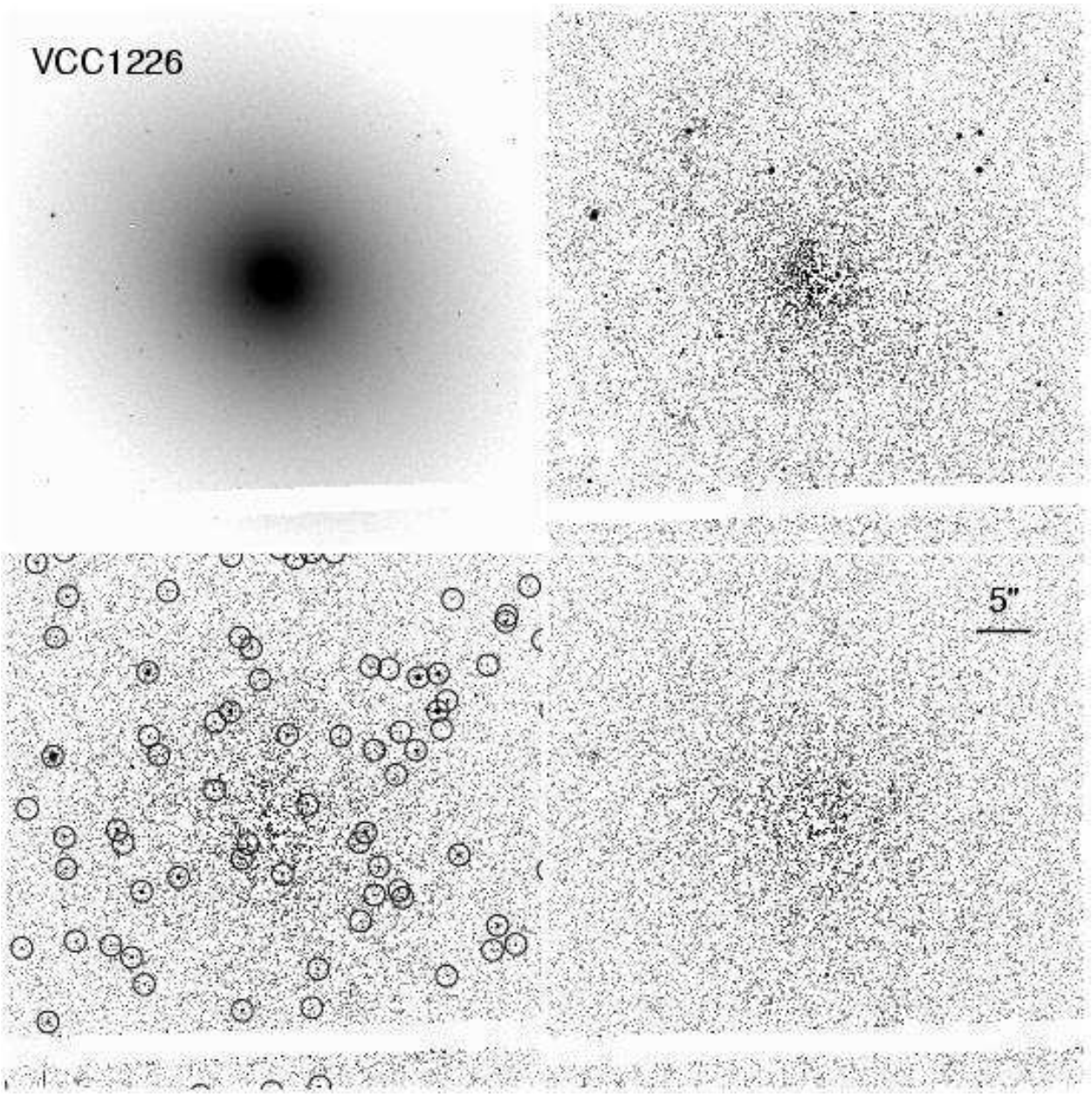

Fig. 6.— An illustration of the various stages in the data reduction pipeline for VCC1226 (M49 = NGC4472), the brightest galaxy in the ACS Virgo Cluster Survey. Each of the four panels shows a $50'' \times 50''$ region centered on the nucleus. *(Upper Left)* Drizzled and co-added F475W image. *(Upper Right)* Image with ELLIPROF model for the galaxy subtracted. Note the large-scale residuals. *(Lower Left)* Image with SExtractor background removed, and sources classified as globular cluster candidates identified. *(Lower Right)* Image after the application of KINGPHOT, with the globular cluster candidates subtracted from the previous image.

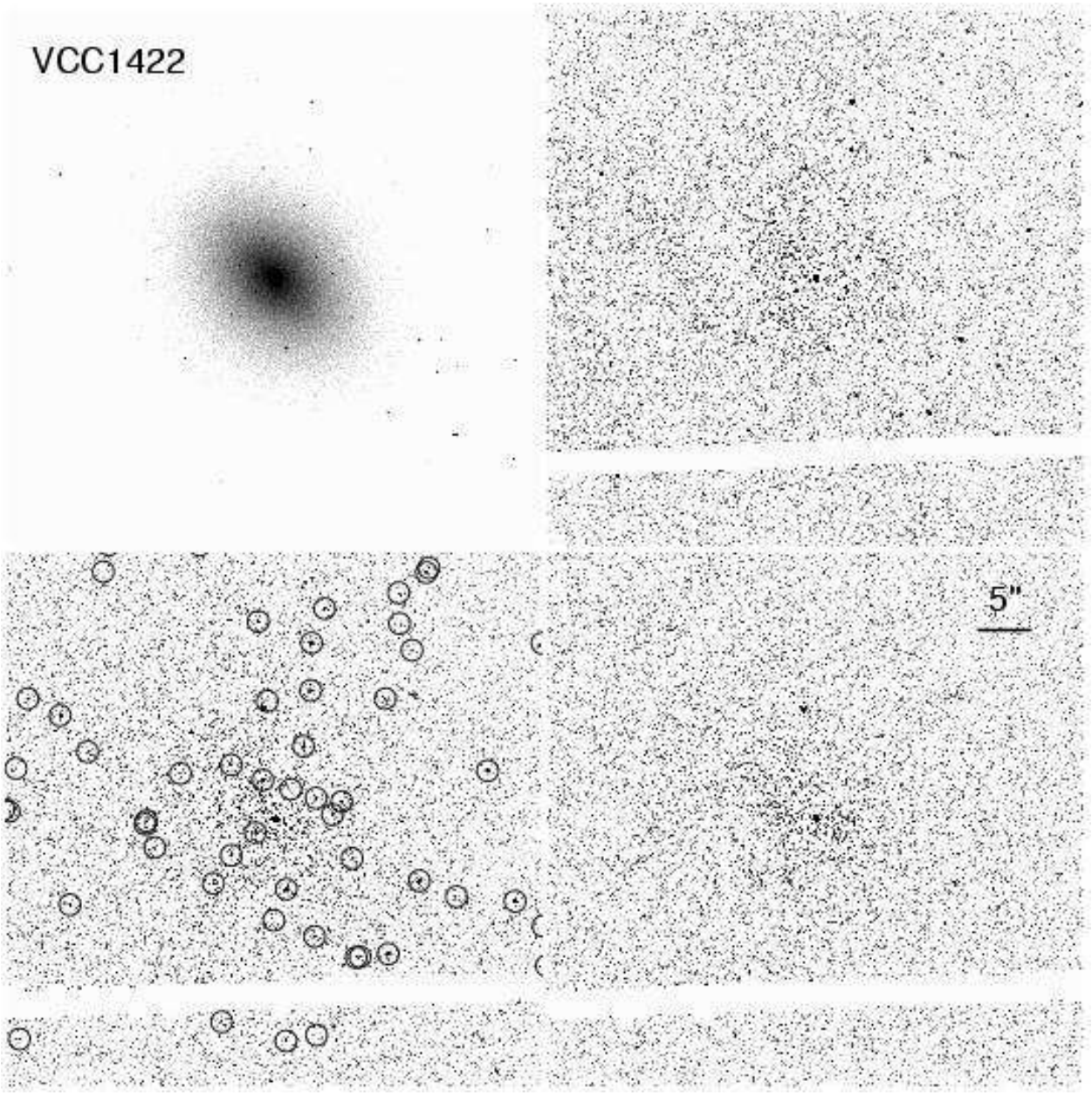

Fig. 7.— Same as Figure 6, except for VCC1422, the 50th brightest galaxy in the survey.

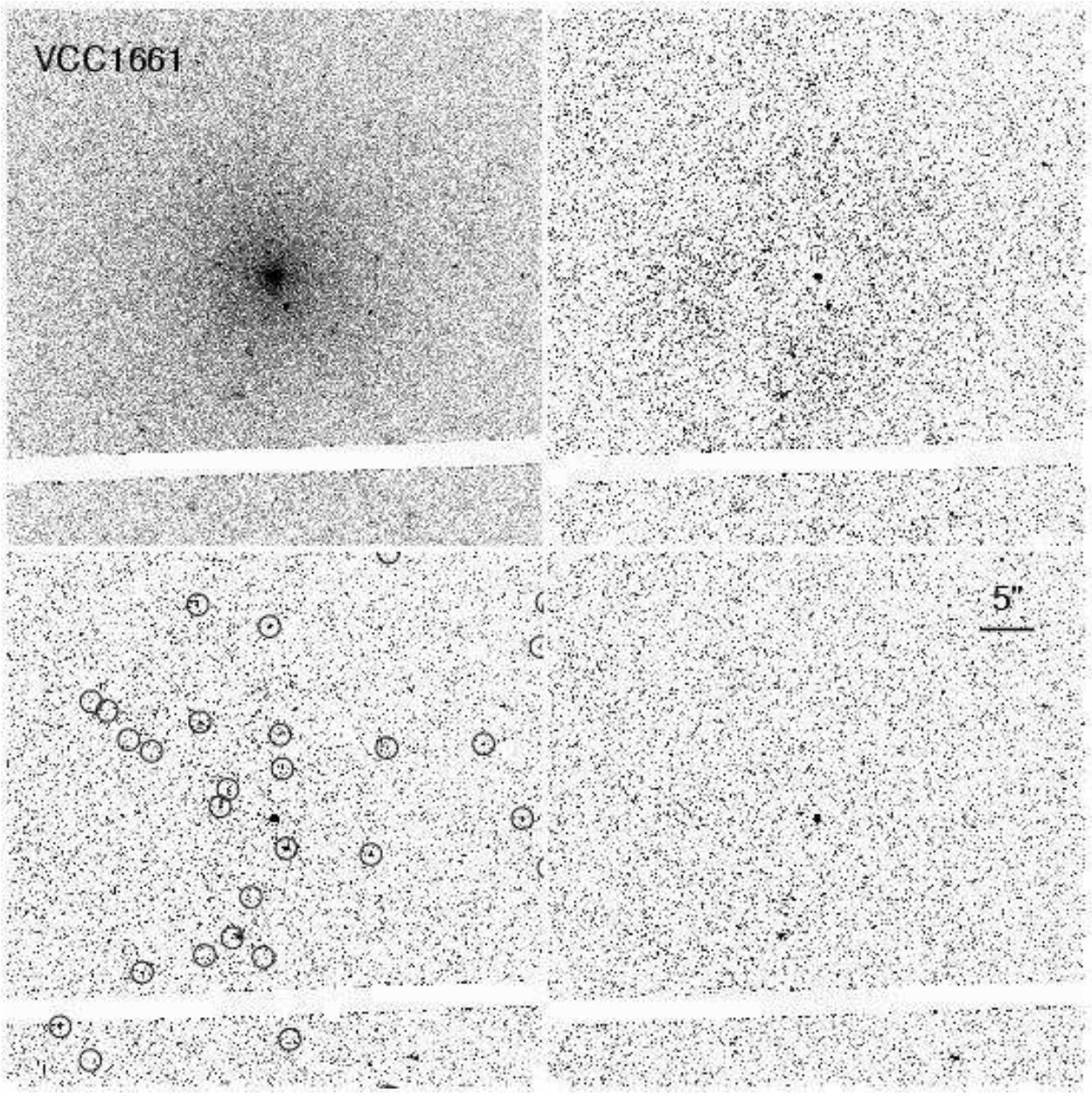

Fig. 8.— Same as Figure 6, except for VCC1661, the faintest of the 100 galaxies in the survey.